RSC Advances

ROYAL SOCIETY OF CHEMISTRY

www.rsc.org/advances

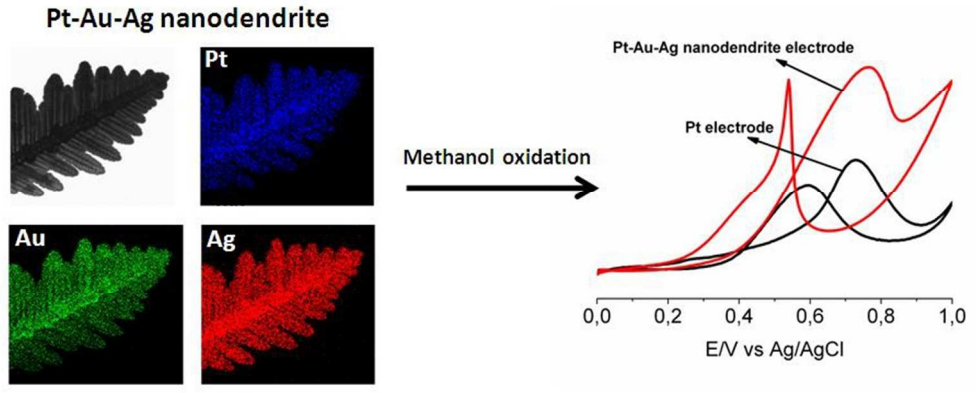

242x97mm (96 x 96 DPI)

Cite this: DOI: 10.1039/c0xx00000x

www.rsc.org/xxxxxx

ARTICLE TYPE

Forest of Pt-Au-Ag tri-metallic nanodendrites as an efficient electrocatalyst for methanol oxidation reaction

Tran Ngoc Huan,[a] Dipak V. Shinde,[a] Saetbyeol Kim,[a] Sung-Hwan Han,[a] Vincent Artero,[b] Hoeil Chung[a]*

Received (in XXX, XXX) XthXXXXXXXXX 20XX, Accepted Xth XXXXXXXXX 20XX

DOI: 10.1039/b000000x

Forests of trimetallic nanodendrites composed of Pt, Au, and Ag have been synthesized and their catalytic performances with regard to the methanol oxidation reaction (MOR) were evaluated. Analysis based on elemental mapping revealed homogeneous incorporation of Pt, Au, and Ag throughout the nanodendrite and single crystalline structure. These materials proved active for MOR, with improved electrocatalytic performances with regards to Pt in terms of both over potential and stability.

Direct methanol fuel-cells hold promise as fuel-cell technology because of their compactness and use of a liquid fuel. Platinum is an important component in anode electrocatalyst in polymer electrolyte membrane direct methanol fuel cells (PEM-DMFCs).[1-14] Diverse Pt-incorporating multi-metal nanostructures such as nanoparticles, core-shells, and nanowires have recently been reported and demonstrated to be efficient electrocatalysts for fuel cell application,[1-29] and of their applications is methanol oxidation reaction (MOR).[1,2,24,25,30] Here we report a novel Pt- and Au-incorporated Ag nanodendrite structure with significantly improved catalytic activity for MOR.

Among Pt-incorporated multi-metal materials, Pt-Au nanostructures have superior catalytic performance because the incorporated Au suppresses the adsorption of poisoning species, thereby improving stability during catalytic reactions.[24-29] A Pt-Au nanostructure with an ultra-high surface area and large number of active sites would be expected to have excellent catalytic activity. Meanwhile, nanodendrites have attracted interest as hierarchical nanostructures with a high population of edges as well as acute angles in terraces, thereby providing a high surface-to-volume ratio and a large number of active sites.[31-34] For example, we previously described the fabrication of a three dimensional (3D) Au nanodendrite structure that could electrochemically detect arsenic concentrations as low as 0.1 ppb because of its large surface area. In this research, we first fabricated a Ag nanodendrite forest by galvanostatic electrodeposition of Ag^+ on a Ti substrate (1×1 cm^2) in a 10 mM citric acid solution. A scanning electron microscope (SEM) image of the resulting structure is shown in Figure 1, with the inset figure showing a magnified image of a single nanodendrite. Individual Ag nanodendrites can be easily identified with characteristic terraces aligned along the dendrite column. In a second step, Pt and Au were incorporated into the pre-built Ag nanodendrites using GRR methods. Because the Ag nanodendrite forest was constructed as a physical frame for subsequent incorporation of both metals, its structure directly determines the total surface area of the final trimetallic nanodendrite.

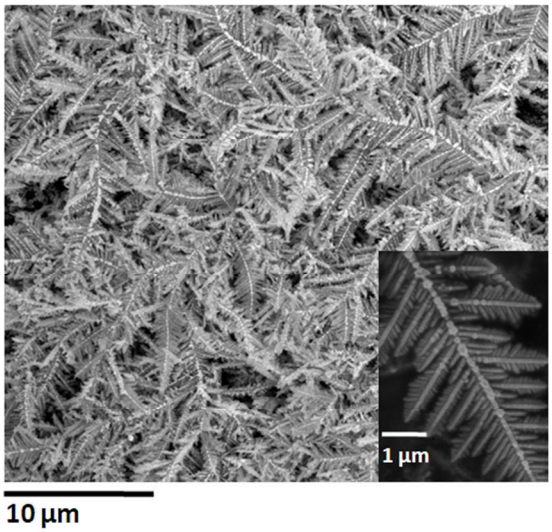

Fig. 1 SEM image of a Ag nanodendrite forest formed on a Ti electrode via electrodeposition of Ag^+. A single nanodendrite clearly showing characteristic terraces aligned along a dendrite column is shown in the inset.

Fabrication of trimetallic Pt-Au-Ag was performed based on the fact that the standard redox potential of the Ag^+/Ag couple (0.8 V vs. SHE) is lower than that of the Pt^{2+}/Pt (1.2 V) and Au^{3+}/Au (1.5 V), thus making the two GRRs (1) and (2) thermodynamically favorable, and allowing for simultaneous incorporation of both metals into Ag nanodendrites.

$$4Ag + AuCl_4^- \rightleftharpoons Au + 4AgCl \quad (1)$$

$$4Ag + PtCl_4^{2-} \rightleftharpoons Pt + 4AgCl \quad (2)$$

Transmission electron microscope (TEM) image of a single Pt-Au-Ag nanodendrite is shown in Figure 2 (a). A dendritic structure is apparent without any indication of structural deformation after the GRRs. Elemental mapping of Pt (blue), Au (green), and Ag (red) was performed separately for the same

nanodendrite, and the results are shown in Figs 2 (b), (c), and (d), respectively. Each color was uniformly distributed over the structure, demonstrating homogeneous incorporation of Pt and Au throughout the nanodendrite. The determined atomic percentages of Pt, Au, and Ag based on the EDAX measurements on the resulting nanodendrite were 21.0, 38.0, and 41.0%, respectively.

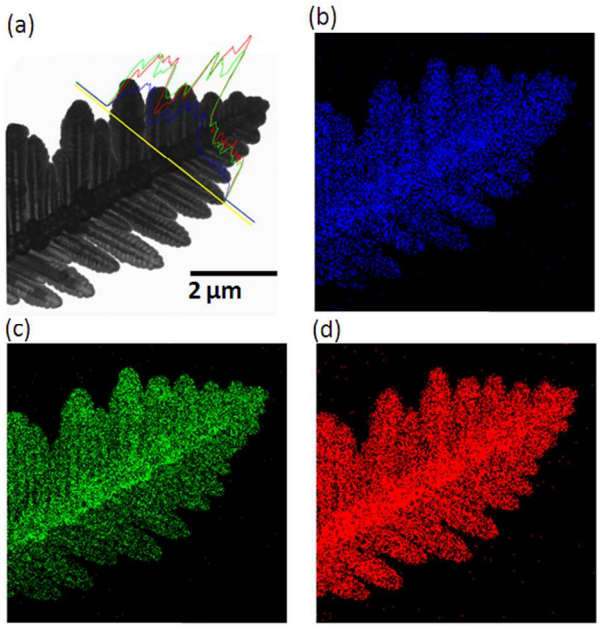

Fig. 2 TEM image of a single Pt-Au-Ag nanodendrite (a) composed of 21.0% Pt, 38.0% Au, and 41.0% Ag. Line mappings that cross the pivot of the nanodendrite are overlaid on the image. Blue, green, and red indicate intensity variations of Pt, Au, and Ag, respectively. Elemental mappings of Pt (blue, (b)), Au (green, (c)), and Ag (red, (d)) performed separately for the nanodendrite are also shown.

This is further supported by line mapping crossing the pivot of the nanodendrite and terrace. Fig. 2 (a) shows overlaid line maps on the corresponding TEM image. Again, blue, green, and red traces indicate the intensity variation of Pt, Au, and Ag, respectively, along the mapping line. The intensities of these three metals varied almost synchronously, confirming the homogeneous tri-metal composition of the nanodendrite. The higher intensity of Au than that of Pt indicates that replacement of Ag by Au is faster than that of Ag by Pt when the concentrations of $PtCl_4^{2-}$ and $AuCl_4^-$ used during GRRs are equal (5 mM), due to the higher redox potential of the Au^{3+}/Au couple.

One of the advantages of using competitive GRRs is that the atomic concentrations of each metal in a nanodendrite can be easily controlled by changing reaction conditions such as the reagent concentration and reaction time. Hence, we could tune the composition of the trimetallic nanodendrite by increasing or decreasing the concentration of $PtCl_4^{2-}$ and $AuCl_4^-$, and thereby obtain nanodendrites with up to 20.0% Pt and 46.0% Au or 57.0% Pt and 14.0% Au respectively. (Preparation details and characterization are provided in the SI and Fig. S1-S2).

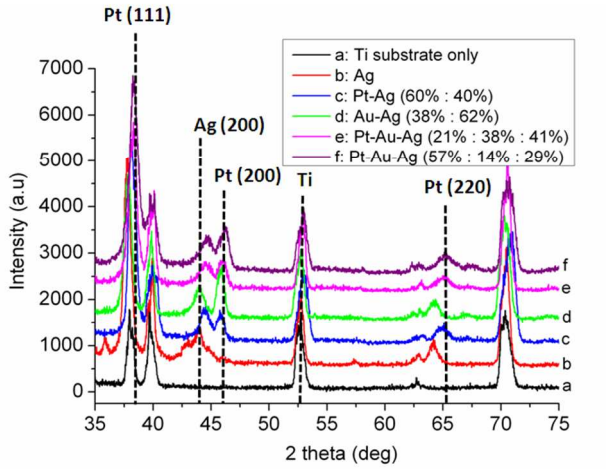

Fig. 3 XRD patterns of samples prepared by increasing the number of metal components in the structure: (a) Ti, (b) Ag nanodendrite, (c) Pt-Ag nanodendrite, (d) Au-Ag nanodendrite, (e) Pt-Au-Ag nanodendrite (21.0% Pt : 40.0% Au : 38.0% Ag), and (f) Pt-Au-Ag nanodendrite (57.0% Pt : 14.0% Au: 29.0% Ag).

To examine the crystal structure of the Pt-Au-Ag nanodendrites, we performed X-ray diffraction (XRD) analysis of samples synthesized by increasing numbers of metal components. The XRD pattern of the Ag nanodendrite was measured as shown in Figure 3. For comparative purposes, the XRD pattern of a Ti substrate is also displayed (Fig. 3, trace a) because its features could overlap with those of the nanodendrites constructed on it. The XRD features of Ag (Fig. 3, trace b) indicate that Ag nanodendrites are formed on the Ti substrate. To investigate variations in the crystalline structure of Ag nanodendrites upon incorporation of either Pt or Au, both Pt-Ag (60.0% Pt and 40.0% Ag) as well as Au-Ag (38.0% Au and 62.0% Ag) bimetallic nanodendrites were individually prepared and the corresponding XRD patterns were obtained. TEM image of the Pt-Ag nanodendrite and the corresponding elemental mappings are shown in Figure S3; Pt and Ag had a homogenous distribution. In the XRD pattern of the Pt-Ag nanodendrite (Fig. 3, trace c), peaks corresponding to Pt (200) and Pt (220) appeared at 46.0° and 65.2°, respectively, while peaks of Pt (111) overlapped with those of Ag (111). In the XRD pattern of the Au-Ag nanodendrite (Fig. 3, trace d), a peak at 45.8° corresponding to Au (200) was apparent and located near the neighboring Ag (200) peak at 43.8°. An evidence for the replacement reaction of Pt is the peak assigned to Ag (200) that was shifted to higher 2theta angles, which might be related to the formation of Pt-Ag alloy with the Pt-Ag distance differing from the Ag-Ag distance. The shifting of Ag (200) peak is actually not clearly observed in the case of Au-Ag, but this effect is seen for the Ag (111) peak (Figure S8). This is in agreement with other previous reports.[35] The XRD patterns of the Pt-Ag and Au-Ag nanodendrites were generally similar to each other, confirming that the replacement of Ag by either Pt or Au does not seriously perturb the original atomic crystalline structure of the Ag nanodendrite. The slight differences in the peak positions are likely due to differences in the lattice distance due to replacement of Ag atoms with atoms of different sizes. XRD spectra were collected for trimetallic Pt-Au-Ag nanodendrites with atomic compositions of 21.0%Pt: 38.0%

Au: 41.0% Ag (Fig.3, trace e) and 57.0% Pt : 14.0% Au: 29.0% Ag (Fig. 3, trace f). The XRD patterns of both trimetallic nanodendrites were largely similar to that of the Pt-Ag nanodendrite (Fig.3, trace c). These observations confirm that there were no substantial changes in the crystal structure after the inclusion of both Pt and Au, again indicative of one-to-one atomic replacement without a change in the original Ag crystalline structure.

Selected area electron diffraction (SAED) and high-resolution TEM (HRTEM) images of the trimetallic nanodendrite composed of 21.0% Pt, 38.0% Au, and 41.0% Ag present in Fig. 2 (a) are shown in Figures S4 (a) and (b), respectively. The SAED patterns clearly verified the presence of a single crystalline structure and the formation of a single phase fcc structure in which Ag atoms were partially replaced by either Pt or Au atoms. The lattice structure is clearly apparent in the HRTEM image, and the parallel lines indicate uni-directional arrangement of crystalline Pt-Au-Ag with an inter-distance of 0.236 nm. We finally explored the optimal atomic composition of trimetallic nanodendrites for catalytic methanol oxidation and compare our materials with bare Pt and Pt-Ag (82.6% Pt and 17.4% Ag) nanodendrite structures. We then explored different compositions of trimetallic (Pt:Au:Ag) nanodendrites designated as Pt-Au-Ag-1(38.0% : 3.8% : 58.2%), Pt-Au-Ag-2(60.6% : 5.1% : 34.3%), Pt-Au-Ag-3(75.3% : 6.1% : 18.6%).

Figure 4(a) shows polarization curves corresponding to MOR measured in aqueous solution containing 0.5 M methanol and 0.2 M H_2SO_4 using the different catalyst structures (Corresponding CVs of MOR in Figure S5). All measurements were normalized by the corresponding electrochemically active surface areas (EASAs, See the Supporting Information, Figure S6),[1,2,15,24] which was obtained by dividing the charge for a monolayer of adsorbed hydrogen (Q_H) on the electrode surface by the charge of the adsorbed hydrogen monolayer (Q_S) per unit area (cm^2). The area of the electrode surface was 1×1 cm^2 as described. As shown in Fig. S6 (b), the EASAs of Pt-Au-Ag nanodendrite forest electrodes are up to 6 times higher than bare Pt electrode for the same geometric surface area, a marked advantage for the preparation of highly active MOR electrodes. A bare Ti and Ti-Ag nanodendrite electrode has been also tested for MOR, and these electrodes were not activity for the measurement.

After normalization for the active surface area, the intensity of the electrochemical signal acquired from the bare Pt (a) was lower than those obtained using the other bi- or tri-metallic nanodendrite structures. This demonstrates the enhanced catalytic activity, indicating synergetic effects between metallic elements such as activation or trapping of reactive intermediates. The trimetallic nanodendrite material Pt-Au-Ag-3 displays the highest electrocatalytic current in the series and methanol oxidation peak potential is almost identical to that obtained from the bare Pt electrode. Pt-Au-Ag nanodendrite materials with higher Pt loadings do not display a better activity, indicating that surface Pt loading is already maximized in Pt-Au-Ag-3 and that additional Pt was incorporated inside the structure, therefore not contributing to catalysis. Overall, the Pt-Ag nanodendrite displays poorer MOR activity as compared to Pt-Au-Ag-3 despite slightly higher peak intensity but a more negative potential.

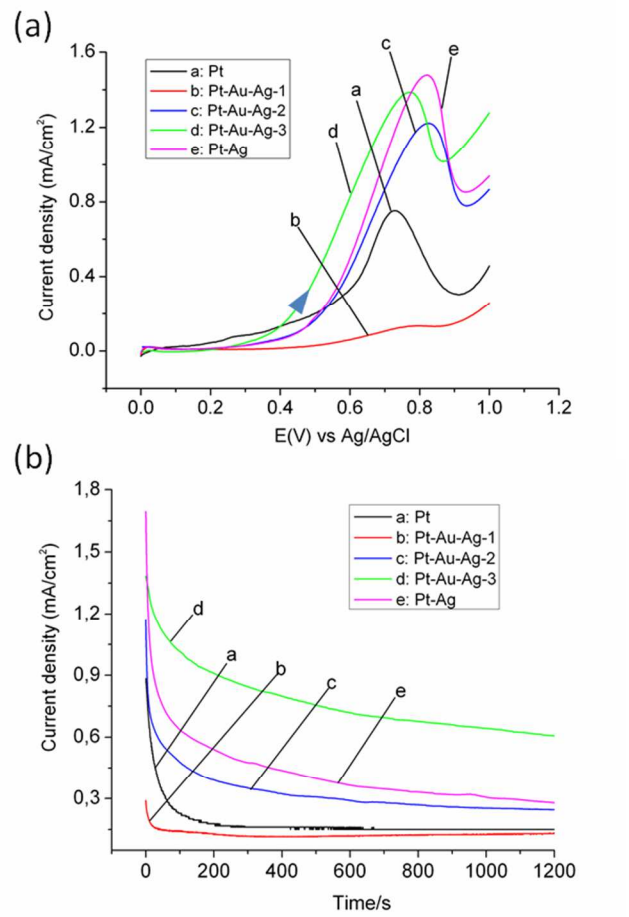

Fig. 4 Polarization curves of MOR (a) acquired in an aqueous solution containing 0.5 M methanol and 0.2 M H_2SO_4 (scan rate: 50 mV/s) using five different structures. Pt-Au-Ag-1, Pt-Au-Ag-2, and Pt-Au-Ag-3 refer to trimetallic nanodendrites composed of 38.0% Pt: 3.8% Au : 58.2% Ag, 60.6% Pt : 5.1% Au : 34.3 % Ag, and 75.3% Pt : 6.1% Au : 18.6% Ag, respectively. Variations in current density during MOR over 1200 seconds were measured at 0.7 V vs Ag/AgCl using the same five structures are also shown (b).

Fig. 4(b) shows the variations in MOR current density over 20 minutes measured on the same electrode materials as a potential of 0.7V vs Ag/AgCl. When the Pt-Ag nanodendrite was used, the signal was initially high but dramatically decreased within the initial 200s. This decrease in catalytic activity is attributed to surface poisoning caused by the adsorption of intermediate species. In contrast, when the Pt-Au-Ag-3 nanodendrite was used, the decrease in current density during MOR was much less significant and superior catalytic performance was maintained even after 20 minutes. The relative decrease in current during the initial 200 seconds when using the Pt-Ag and Pt-Au-Ag-3 catalysts was 65% and 30%, respectively, compared to 83% for the bare Pt catalyst. As expected, the Pt-Au-Ag-1 and Pt-Au-Ag-2 catalysts had inferior catalytic activity and stability than those of Pt-Au-Ag-3. To further attest the activity of Pt-Au-Ag-3, CVs of this electrode were recorded before and after 20 min. of catalytic activity (Fig. S7). The reduction peak of Pt as well as the peak of hydrogen adsorption-desorption are not modified, which confirms the stability of the material during MOR.[36,37] The

catalytic stability of Pt-Au-Ag-3 for MOR reaction has been significantly increased by comparison with previous reports on MOR-active materials: for example bi-metallic Pt-Au materials exhibit a 57% degradation of catalytic activity after 1200s of MOR reaction.[12]Pt-Au-Ag-3 also performs better than other bi- or tri-metallic alloys incorporating Pt and other metals, such as Zn, Fe orPd.[2,15,16]

Conclusions

The nanodendrite forest structures composed of Pt, Au, and Ag have been reported in this research. The trimetallic nanodendrite shows excellent MOR catalytic activity as compared to bare Pt electrodes by providing larger active surface area. Importantly, our results indicate that incorporation of an appropriate amount of Au in a tri-metallic nanodendrite substantially enhances its stability during MOR. Competitive GRRs allowed us to easily control the atomic composition of the structure. Such a versatile synthetic method can be applied to develop other original nano-catalysts.

Notes and references

[a]*Department of Chemistry, College of Natural Science, Hanyang University, Seongdong-Gu, Seoul, Korea, 133-791, Republic of Korea E-mail: hoeil@hanyang.ac.kr*
[b]*Laboratory of Chemistry and Biology of Metals, Université Grenoble-Alpes, CNRS, CEA, 17 rue des Martyrs, 38054 Grenoble cedex 9, France*

Acknowledgements

This research was supported by the Basic Science Research Program through the National Research Foundation of Korea (NRF) funded by the Ministry of Education, Science and Technology (2012R1A1B3003965).

† Electronic Supplementary Information (ESI) available: [details of any supplementary information available should be included here]. See DOI: 10.1039/b000000x/

1 W. Zhang, J. Yang, X. Lu, *ACS Nano* 2012, 6, 7397-7405.
2 Y. Kang, J.B. Pyo, X. Ye, T.R. Gordon, C.B. Murray, *ACS Nano* 2012, 6, 5642-5647
3 T. Iwasita, F. C. Nart and W. Vielstich, Ber. Bunsen-ges. *Phys. Chem*. 1990, 94, 1030.
4 N. Markovic, H. A. Gasteiger, P. N. Ross, L. Villegas andM. J. Weaver, *Electrochim. Acta* 1995, 40, 91.
5 H. A. Gasteiger, N. Markovic, P. N. Ross and E. J. Cairns, *J. Electrochem. Soc*. 1994, 141, 1795.
6 T. Iwasita, H. Hoster, A. John-Anacker, W. F. Lin and W. Vielstich, *Langmuir* 2000, 16, 522.
7 H. Hoster, T. Iwasita, H. Baumgartner and W. Vielstich, *Phys. Chem. Chem. Phys*. 2001, 3, 337.
8 H. Hoster, T. Iwasita, H. Baumgartner and W. Vielstich, *J.Electrochem. Soc*. 2001, 148, A496.
9 D. Kardash, C. Korzeniewski and N. Markovic, *J. Electroanal. Chem*. 2001, 500, 518.
10 M. Krausa and W. Vielstich, *J. Electroanal. Chem*. 1994, 379, 307.
11 W. Chrzanowski and A. Wieckowski, *Langmuir* 1998, 14, 1967.
12 W. Chrzanowski, W. H. Kim and A. Wieckowski, *Catal. Lett*. 1998, 50, 69.
13 G. Tremiliosi-Filho, H. Kim, W. Chrzanowski, A. Wieckowski, B. Grzybowska and P. Kulesza, *J. Electroanal. Chem*. 1999, 467, 143.
14 A. Kabbaby, R. Faure, R. Durand, B. Beden, F. Hahn, J.-M. Leger and C. Lamy, *J. Electroanal. Chem*. 1998, 444, 41.
15 L. Wang, Y. Yamauchi, *Chem. Mater*. 2011, 23, 2457-2465.
16 S. Guo, S. Zhang, X. Sun, S. Sun, *J. Am. Chem. Soc.* 2011, 133, 15354-15357.
17 M.K. Carpenter, T.E. Moylan, R.S. Kukreja, M.H. Atwan, M.M. Tessema, *J. Am. Chem. Soc.* 2012, 134, 8535-8542.
18 M. Shao, K. Shoemaker, A. Peles, K. Kaneko, L. Protsailo, *J. Am. Chem. Soc.* 2010, 132, 9253-9255.
19 D. Wang, Y. Yu, H. L. Xin, R. Hovden, P. Ercius, J.A. Mundy,H. Chen, J.H. Richard, D.A. Muller, F.J. DiSalvo, H.D. Abruña, *Nano Lett.* 2012, 12, 5230–5238.
20 D. Wang, H.L. Xin, R.Hovden, H. Wang, Y. Yu, D.A. Muller, F.J. DiSalvo, H.D. Abruña, *Nature Materials* 2013, 12, 81-87.
21 D.F. Vliet, C. Wang, D. Tripkovic, D. Strmcnik, X.F. Zhang, M.K. Debe, R.T. Atanasoski, N.M. Markovic, V.R. Stamenkovic, *Nature Materials* 2012, 11, 1051-1058.
22 D. Wang, P. Zhao, Y. Li, *Scientific Reports* 2011, 37
23 M.R. Gao, Q. Gao, J. Jiang, C.H. Cui, W.T. Yao, S.H. Yu, *Angew. Chem.* 2011, 123, 5007 –5010
24 Y. Yamauchi, A. Tonegawa, M. Komatsu, H. Wang, L. Wang, Y. Nemoto, N. Suzuki, K. Kuroda, *J. Am. Chem. Soc.* 2012, 134, 5100-5109.
25 L. Wang, Y. Yamauchi, *Chem. Mater*. 2011, 23, 2457–2465
26 Y. Tan, J. Fan, G. Chen, N.Zheng, Q. Xie, *Chem. Commun*. 2011, 47, 11624–11626
27 J.Xu,C. Zhang,X. Wang,H.Ji,C. Zhao,Y. Wang, Z. Zhang, *Green Chem.* 2011, 13, 1914
28 B.N. Wanjala, J. Luo, B. Fang, D. Mott, C.J.Zhong, *J. Mater. Chem.* 2011, 21, 4012–4020
29 Z. Zhang, Y. Wang, X. Wang, *Nanoscale* 2011, 3, 1663
30 Y.X. Chen, A. Miki, S. Ye,H. Sakai, M.Osawa,*J. Am. Chem. Soc.* 2003, 125, 3680-3681.
31 T.N. Huan, T. Ganesh, K.S. Kim, S. Kim, S.H. Han, H. Chung, *Biosens. Bioelectron.* 2011, 27, 183-186.
32 I.Dumitrescu, R.M. Crooks, *PNAS* 2012, 109, 11493-11497.
33 G. Zhang, S. Sun, M. Cai, Y. Zhang, R. Li, X. Sun, Scientific Report 2013, 3, 1526.
34 J.N. Tiwari, K.C. Kemp, K. Nath, RN. Tiwari, H.G. Nam, K.S. Kim, *ACS NANO* 2013, Doi: 10.1021/nn4038404
35 D.H. Chen, C.J. Chen, J. Mater. Chem. 2012, 12, 1557-1562.
36 J.X. Wang, C. Ma, Y.M. Choi, D. Su, Y. Zhu, P. Liu, R. Si, M.B. Vukmirovic, Y. Zhang, R.R. Adzic,*J. Am. Chem. Soc.* 2011, 133, 13551-13557.
37 F. Maillard, L. Dubau, J. Durst, M. Chatenet, J. André, E. Rossinot, Electrochem. Commun. 2010, 12, 1161–1164.